 CMES, vol.44, no.1, pp.97-113, 2009

Investigation of Inherent Deformation in Fillet Welded Thin Plate T-joints Based on Interactive Substructure and Inverse Analysis Method

Rui Wang[1], Jianxun Zhang[1], Hisashi Serizawa[2] and Hidekazu Murakawa[2]

Abstract: In this paper, the inherent deformation of fillet welded thin plate T-joints is studied. The prediction procedure of inherent deformation consists of three parts: part one, a three dimensional (3D) thermo-elastic-plastic analysis using an in house finite element (FE) code of interactive substructure method (ISM) is utilized to obtain the welding distortions; part two, corresponding experiments are carried out to verify the computational results of ISM; part three, using the verified computational results, the inverse analysis is utilized to evaluate the welding inherent deformation. Based on the results in this study, an inherent deformations database of fillet welded thin plate T-joints with 8 welding materials is developed. Meanwhile, the influence of welding heat input parameter on inherent deformation is discussed. The results show that the prediction procedure of inherent deformation is effectiveness. The inherent deformation is the key parameters to estimate distortion in fillet welded thin plate T-joints by elastic analysis. Welding heat input parameter and material properties have significant influence on welding inherent deformation.

Keywords: Welding distortion, thin plate T-joints, inherent deformation, ISM, inverse analysis, inherent deformation database.

1 Introduction

A fillet weld is the most common welds types used in the fabrication of welding structural members in ship building, pressure vessels, aerospace structures and other industries. Fillet welded T-joints suffer from various welding distortion patterns, such as transverse shrinkage, angular distortion, longitudinal distortion. Distortions induced by welding have significant impact on fabrication accuracy in-

[1] State Key Laboratory for Mechanical Behavior of Materials, School of Materials Science and Engineering, Xi'an Jiaotong University, Xi'an 710049, P.R.China
[2] Joining and Welding Research Institute, Osaka University, 567-0047, Japan

fluencing the quality and productivity of the welded structures and increase the fabrication costs. Various analytical and computational approaches have been developed to predict welding residual stress and distortion in fillet welded structures [Ma, Ueda, Murakawa and Maeda (1995); Teng, Fung and Chang (2001); Camilleri, Mollicone and Gray (2006); Zaeem, Nami and Kadivar (2007); Deng, Liang, and Murakawa (2007)].

In industrial production, a highly efficient technique to predict welding residual stress and distortion is necessary. With modern computing facilities, finite element method (FEM) has become a cost-effective method for prediction and assessment of residual stress and distortion [Lindgren (2001a, 2001b, 2001c); Dong (2005); Raju, Glaessgen, Mason, Krishnamurthy and Davila (2007)]. Recent years, high efficient simulation techniques, including hardware and highly efficient algorithms have been proposed. Oishi and Yoshimura (2008) described the finite element analyses of dynamic problems using graphics hardware (GPU). The results indicate that GPU can perform dynamic finite element analyses faster than CPU. Michaleris and DeBiccari (1997); Deo, Michaleris and Sun (2003) described an efficient numerical technique which combines two-dimensional welding simulation with three-dimensional structural analyses in a decoupled approach. The effectiveness of this approach is verified by experimental results. This method can reduce computational time to evaluate welding induced buckling in large and complex structures. To reduce the computational effort required to achieve reliable solutions, Alaimo, Milazzo and Orlando (2008) proposed global/local FEM-BEM to analyze the fracture mechanics behavior of complex aerospace structures. The accuracy and the effectiveness of the model have been demonstrated analyzing classical stress concentration problems. The simplified FEM to simulate the out-of-plane distortion caused by welding was proposed by Camilleri and Gray (2005), Camilleri, Comlekci and Gray (2005). The simplification deals with the thermal transient process in a simple two-dimensional cross-section model of the welded joint and the thermo-elastic-plastic process is treated based on simple analytical algorithms describing transverse and longitudinal deformation. Based on this method, computational results can be obtained within reasonable computational time. Tsai, Park and Cheng (1999) studied welding distortion behaviors of thin aluminum panel structure using experiment and FE analysis. The essential conditions for plate buckling distortion were determined and the joint rigidity method was proposed to determine the optimum welding sequence for the minimum welding distortion. Murakawa (2007), Nishikawa, Serizawa and Murakawa (2007) proposed a highly efficient FE analysis using an iterative substructure method (ISM). ISM has been developed to transform welding problem into the combination of a large linear region and a small but moving strong nonlinear region. Thus, the computation speed

can be improved greatly. The continuity on the boundary between the linear and the nonlinear regions is maintained through iterative procedure. With Dell Precision 380 workstation (3.8 GHz CPU, 2 G memory), the CPU time consumed by a mechanical analysis of 13778 elements and 16970 nodes is 9000 s [Zhang, Zhang, Serizawa, and Murakawa (2007)]. ISM can be used for computation of welding distortion with large welded structures in short computation time.

As we known, residual stresses and distortions after welding are caused by the cumulative plastic strains (inherent strains) accumulated during plastic deformation. Ueda, Fukuda and Tanigawa (1979) proposed inherent strain method which means that welding-induced distortion could be determined by a linear elastic model if the magnitude and distribution pattern of the inherent strains were known. In fact, inherent strain method has been approved as an efficient and practical approach to analyze the distortion in large and complex structures without performing the thermo-elastic-plastic analysis [Yuan and Ueda (1996); Takeda (2002)]. Seo and Jang (1999) used the finite element method combining the inherent strain theory to predict reasonably the welding detortion of large structures. The results have been supported by the experimental data. Vega, Rashed, Tango, Ishiyama and Murakawa (2008) investigated the influence of multi-heating lines on line heating inherent deformation. The influence of previous heating lines on inherent deformation of overlapping, parallel and crossing heating lines was clarified. The proximity to plate side edge on inherent deformation was also taken into account in the analysis. However, few studies on welding inherent deformations in fillet welded thin plate T-joints for different materials have been reported. Therefore, understanding the characteristic of inherent deformation in thin plate T-joints, creating the database of inherent deformation, and utilizing the inherent deformation database to prediction the distortion in large and complex structures without performing the thermo-elastic-plastic analysis are indeed necessary for engineering application.

In this study, welding inherent deformation was studied according to three procedures. First, three dimensional (3D) thermo-elastic-plastic finite element analyses using an ISM was used to predict welding distortion of fillet welded T-joint. Second, the effectiveness of the simulation result was confirmed by the experimental results. Then, incorporating welding distortion, inverse analysis technique was performed to obtain the welding inherent deformation database. Based on the studies above, the influence of welding heat input parameters and material properties on inherent deformation were discussed.

2 Experimental procedure

The fillet welded T-joints were made of SUS304 stainless steel and SS400 carbon steel. The filler wires were GFW308L and MGS-50, respectively. The welding

method was CO_2 gas metal arc welding. The experimental results were used to verify the FE model. The following works can be done with welding experiments:

(1) To continuously measure temperatures during welding and cooling, using thermocouples in fixed positions along the direction perpendicular to weld bead on the specimens (distance from the weld centerline: 10 mm, 20 mm, and 30 mm).

(2) To measure the middle section configurations of the T-joints.

(3) To measure the welding distortion including, transverse shrinkage, angular distortion and longitudinal shrinkage of the welded specimens on top and bottom surfaces.

During the welding process, two-pass welds were implemented. After the first pass welding, the specimen cooled down to the ambient temperature. The experimental set-up is shown in Fig.1, and the supporting condition is shown in Fig.2. The size of fillet welded T-joint used in the experiment is 200 mm $\times$ 200 mm for the flange and 200 mm $\times$ 50 mm for the web with different thickness. Welding parameters were adjusted among the experiments to yield a high quality weld. The thickness of specimens and welding conditions are given in Tab.1.

Figure 1: Experimental set-up of fillet welding

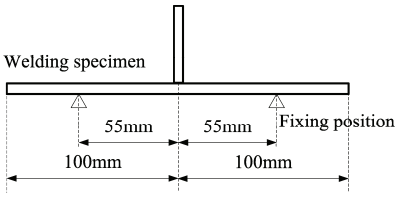

Figure 2: Schematic illustration of supporting condition

3 3D thermo-elastic-plastic FE analysis procedure

The thermo-mechanical behavior of the weldment during welding was simulated using an uncoupled method. The solution procedure was consisted of two steps.

Table 1: Welding condition

Welding material	Thickness of flange plate and web plate (mm)	Current (A)	Voltage (V)	Speed (cm/min)	Wire feed rate (mm/s)
SS400 (first pass)	6.0 (flange) - 4.5 (web)	180	24	30	69
SS400 (second pass)	6.0 (flange) - 4.5 (web)	175	24	30	69
SUS304 (first pass)	6.0 (flange) - 5.0 (web)	140	28.5	35	88
SUS304 (second pass)	6.0 (flange) - 5.0 (web)	135	28.5	35	87

First, the temperature distribution and its history in the welding model were computed by the thermal analysis. Then, the thermal analysis results were employed as a thermal load in the subsequent mechanical analysis. The same finite element model used in the thermal analysis was employed in the mechanical analysis. The base materials and filler materials were assumed to have the same material properties.

3.1 Thermal analysis

In order to predict distortion patterns induced by welding, it is critical to obtain a reasonable temperature evolution without the significant loss of accuracy. In the thermal analysis, the heat from the moving welding arc was applied as a uniform moving volumetric heat source. The appropriate heat generation rate was achieved by manual adjustment of the parameters and compared with the pre-designed fillet profile. The heat generation rate h_{gen} was constant over the moving heating length, which was formulated as follows:

$$h_{gen} = \frac{UI\eta}{V} \tag{1}$$

where U is the voltage, I is the current, η is the arc efficiency and V is the heating volume. The total heat input Q of each heating length is determined by

$$Q = h_{gen}\frac{L}{v} \tag{2}$$

where h_{gen} is heat generation rate, v is the traveling speed of welding arc and L is the moving heating length which was specific as 20 mm in this study.

The effectiveness of the thermal analysis results can be validated by comparing the temperature results at given positions with the experimental results and also comparing the middle section shape from the weld tests with the predicted boundary of the molten pool.

3.2 Elastic-plastic mechanical analysis method

The main purpose of elastic-plastic mechanical analysis in the study was to obtain the welding distortions including transverse shrinkage, longitudinal shrinkage, and angular distortion for fillet welded thin plate T-joints. The ISM was adopted during the analysis to predict welding distortion. The ISM extracted the strongly non-linear region from the whole weakly non-linear region and reduced the number of solving large matrix associated to the latter.

3.3 FE model

Fig.3 shows the finite element models used in the thermal and mechanical analysis. The quadratic brick elements were used in this model. The total number of elements and nodes were 14400 and 18309, respectively. The size of fillet welded T-joints and welding process parameters were the same as those used in the experiments. Three nodes on bottom surface of the flange plate (Y = 45 mm, X = 0 mm and X = 200 mm as well as Y = 155 mm, X = 0 mm) were constrained during welding and cooling to simulate the supporting condition (see Fig.2).

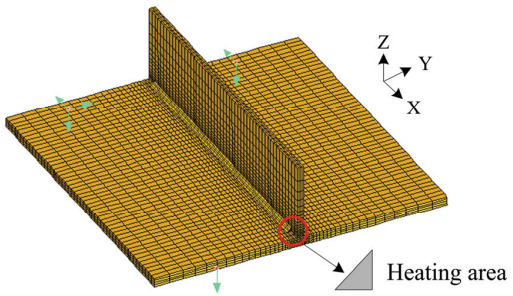

Figure 3: Finite element model

3.4 Material model

Generally speaking, welding distortion depends on geometry shape, welding conditions, and material properties. During the computation in this study, temperature-dependent thermo-physical and mechanical properties of SUS304 stainless steel and SS400 carbon steel in both thermal analysis and mechanical analysis were considered. The thermo-physical and mechanical properties of two materials are shown in Fig.4.

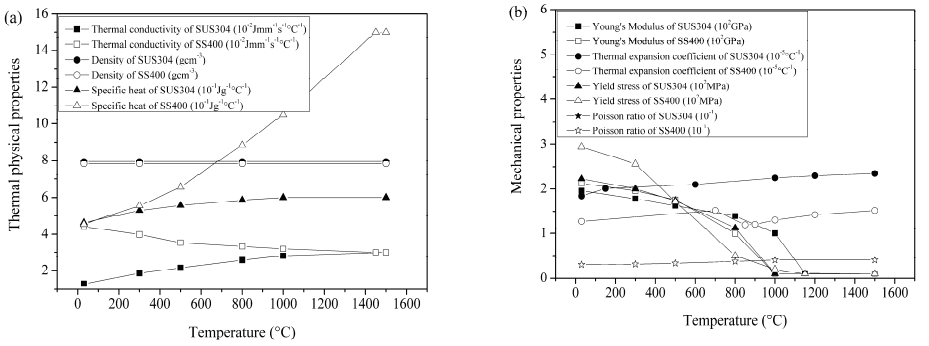

Figure 4: Temperature-dependent material properties (a) Thermal physical properties, (b) Thermal mechanical properties

3.5 Computational results and discussion

Welding temperature and distortion results including transverse shrinkage, angular distortion, and longitudinal shrinkage were predicted and compared with the experimental results.

The temperature histories were measured by thermocouples along the line perpendicular to weld centerline. The comparison between the temperature histories (the second pass welding) obtained by computational and experimental are shown in Fig.5 (a) and (b), respectively.

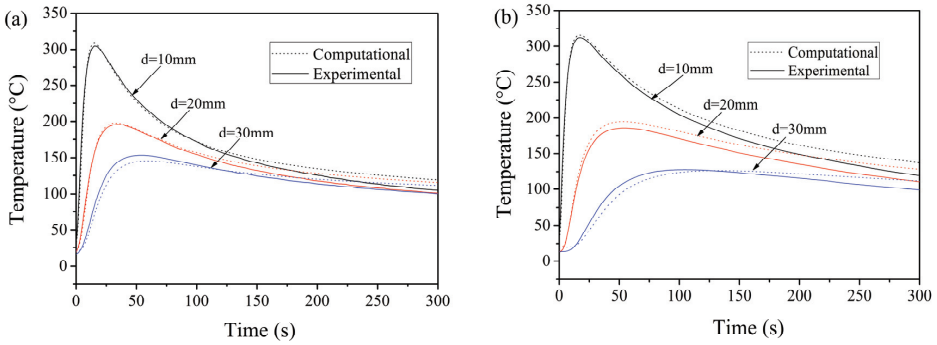

Figure 5: Temperature histories of the second pass (a) SS400 carbon steel, (b) SUS304 stainless steel

From Fig.5, it can be seen that the agreement between temperature histories of computations and experiments is good at all positions. The cooling rates, peak temperatures of the computational results agree well with the experimental results.

The computational procedures were based on the optimum conditions of the experiments such as arc efficiency, heat source power, and heat losses. Fig.6 shows the computational results of fusion boundaries. From the results, it can be concluded that the prediction results capture the overall dimensions of the fusion boundaries and the overall macro-section shapes obtained by computations and experiments are identical. In addition, the results validate the effectiveness of thermal analysis.

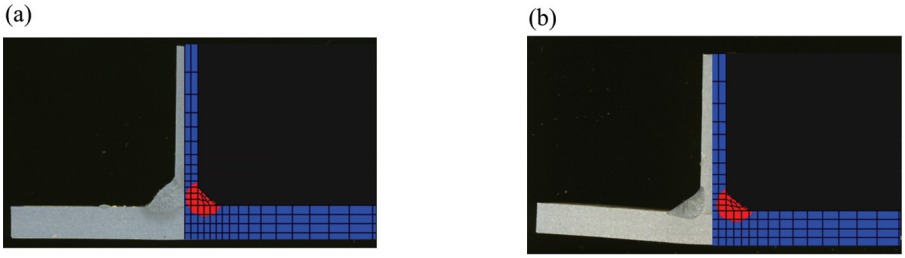

Figure 6: Macro-section of fillet welding T-joints (a) SS400, (b) SUS304

The computational and experimental results of welding distortions are shown in Figs.7–9. Fig.7 shows the computational and experimental results of transverse shrinkage. It is evident that experimental and computational results of transverse shrinkage are in good agreement on top and bottom surfaces. The transverse shrinkage of the plate centre is larger than those of the two sides. The results mean that a bending shrinkage is produced after welding, and the plates show a little camber bending along welding direction.

Fig.8 shows the results of angular distortion between experiments and computations. The computational results of angular distortion are in good agreement with experimental results. In simple supporting condition, the angular distortion increases along welding direction.

The results of longitudinal shrinkage are shown in Fig.9. We can see that the FE model can successfully predict the magnitude and trends of longitudinal shrinkage even the magnitude of longitudinal shrinkage is small. The longitudinal shrinkage near the weld zone is larger than these of two sides of specimens, which means longitudinal shrinkage is notably happened in the weld zone. However, there is little longitudinal shrinkage produced far away from the weld bead.

From the results shown in Figs.7-9, it can be concluded that the welding distor-

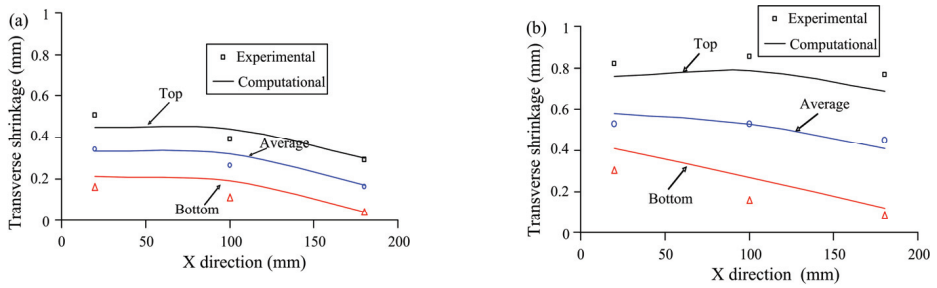

Figure 7: Transverse shrinkage (a) SS400, (b) SUS304

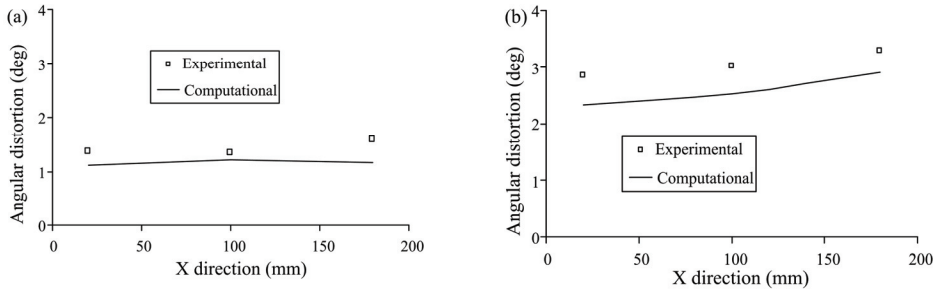

Figure 8: Angular distortion (a) SS400, (b) SUS304

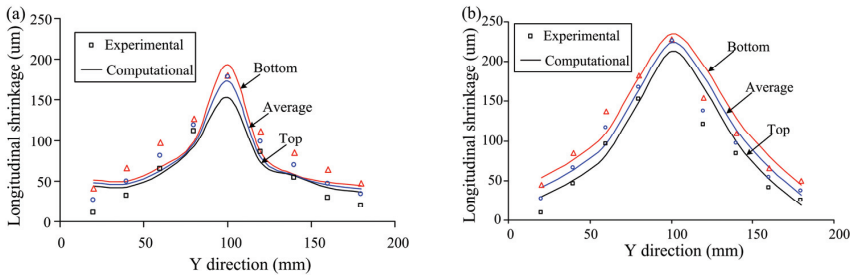

Figure 9: Longitudinal shrinkage: (a) SS400, (b) SUS304

tion of SUS304 stainless steel is larger than SS400 carbon steel. The heat inputs (Q/h^2) for these two cases are 34.35 and 34.07 J/mm^3, respectively. Under the similar welding heat input, temperature-dependent material properties play an important role on welding distortion as reported by McDILL and Oddy (1990), Zhu and Chao (2002). The yield stress and Young's Modulus of SUS304 stainless steel

are smaller than those of SS400 carbon steel and the thermal expansion coefficient of SUS304 stainless steel are larger than that of SS400 carbon steel (see Fig.4). The smaller yield stress and Young's Modulus and larger thermal expansion coefficient play an important role in explaining why SUS304 stainless steel distorts more than SS400 carbon steel. The computational results of welding distortion show that the magnitudes and trends of welding distortion between computational and experimental results are matched well. Therefore, welding distortions can be accurately predicted by ISM.

3.6 Elastic FE analysis

Welding distortion is expressed in terms of the inherent deformation which is defined as the integration of the plastic strain over the cross section of the T-joint. Inherent deformation is divided into four components named longitudinal shrinkage, transverse shrinkage, longitudinal bending, and transverse bending. These four components are defined as shown by Eq.3:

$$\begin{cases} \delta_x^i = \int \varepsilon_x^i dydz/h \\ \delta_y^i = \int \varepsilon_y^i dydz/h \\ \theta_x^i = \int \varepsilon_x^i (z-h/2)/(h^3/12) dydz \\ \theta_y^i = \int \varepsilon_y^i (z-h/2)/(h^3/12) dydz \end{cases}$$

where x is welding direction, y is the direction vertical to welding direction, h is the thickness of plate, ε_x^i is the inherent strain in X direction, and ε_y^i is the inherent strain in Y direction.

On the contrary, if the welding distortion at selected points of the model F_j^m was given from the measurements or the thermo-elastic-plastic FE analysis (adopted in this study), the inherent deformation (δ_x^i, δ_y^i, θ_x^i, θ_y^i) can be calculated by solving the following equation using inverse analysis:

$$F_j(\delta_x^i, \delta_y^i, \theta_x^i, \theta_y^i, \cdots) = F_j^m \tag{3}$$

Inverse analysis was described detailed by Liang, Sone, Tejima, Serizawa and Murakawa (2004), Liang, Deng and Murakawa (2005).Using inherent deformations, the welding distortion can be effectively calculated by elastic-shell model. Fig.10 shows the shell model of SS400 carbon steel. The mesh size of the shell model and the constraint condition are the same as the 3D thermo-elastic-plastic FE model.

As an example, the angular distortion contour results of SS400 carbon steel calculated by elastic-shell FE using inherent deformation and calculated by ISM are shown in Fig.11. It can be seen that the angular distortion calculated by elastic-shell

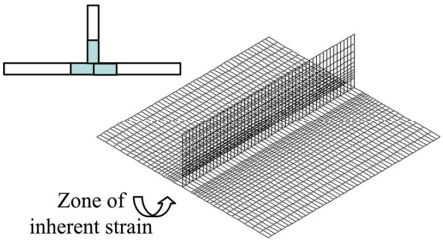

Figure 10: The mesh of shell model

model agrees fairly well with this calculated by ISM. The result indicates that the welding distortion can be accurately predicted by elastic-shell model using inherent deformation.

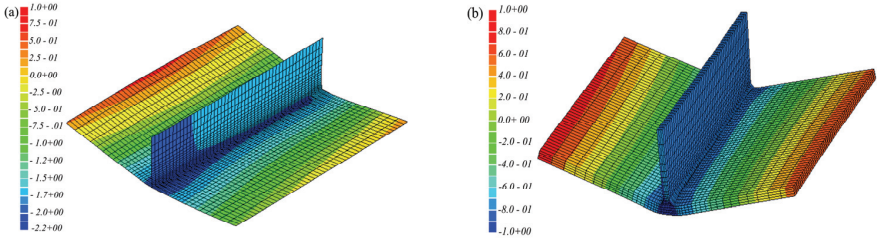

Figure 11: Welding angular distortion computational result (a) Elastic-shell FEM, (b) ISM

4 Inherent deformations of fillet welded T-joint

Inherent deformations was mainly determined by welding heat input, the geometry of welded structure and the type of welded joint [Satoh and Terasaki (1976); Terasaki, Ishimura, Matsuishi and Akiyama (2002)]. As discussed in the section 3.3, welding inherent deformation can be used to accurately predict welding distortion using an elastic-shell model in the given welding condition. Therefore, inherent deformation is the key parameters in estimating welding distortion by elastic analysis. In this section, the inherent deformation with different welding conditions is presented. In addition, the influence of materials properties (8 different materials) on inherent deformations of fillet welded T-joint is also taken into account in the analysis. Understanding the variation of inherent deformations with different welded conditions is deemed necessary to predict welding distortion of

actual welding structure. The range of welding parameters used in the computation is presented in Tab. 2.

Table 2: The range of computational parameters

Flange plate thickness (mm)	Welding current (A)	Welding voltage (V)	Welding speed (mm/s)	Material
4.5, 5, 6, 8	130-185	24-28.5	5-6	SS400, SUS304, SUS316, SUS430,HT570, HT780, SPH270D, SPH440D

4.1 Computational procedure

In the case of fillet welded as shown in Fig.12, welding heat input is given to both the flange and web. The distribution of heat input in flange and web is given by the following equations, respectively:

$$Q_{web} = \frac{h_w}{2h_f + h_w} Q_{total} = \frac{h_w}{2h_f + h_w}(Q_L + Q_R) \tag{4}$$

Where Q_{total} is total heat input; Q_L and Q_R are the heat input in left side and right side of fillet welded T-joint, respectively; h_w and h_f are the thickness of web and flange, respectively.

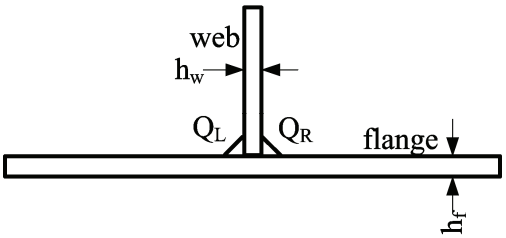

Figure 12: Heat input distribution in fillet welding joint

According to Eqs.5 and 6, the heat input in the flange and web is different. Therefore, the inherent deformation of the web and flange was calculated separately. The relationship of inherent deformations versus welding conditions can also be defined as the relationship between inherent deformation versus heat input parameter Q/h^2.

4.2 Effects of heat input parameter on inherent deformation

The computational results of inherent deformation in the flange and web of fillet welded T-joints are shown in Figs.13 and 14, respectively.

Fig.13 shows that the inherent deformation (transverse shrinkage (TS), longitudinal shrinkage (LS), transverse bending (TB), and longitudinal bending (LB)) of the flange increases linearly with the increase of Q_{flange}/h_f^2. Transverse shrinkage is larger than longitudinal shrinkage and longitudinal bending is larger than transverse bending. The results mean that the transverse shrinkage and longitudinal bending distortion are prone to happen in fillet welded T-joints when the heat input is in the range of 10–70 J/mm^3.

From the computational results, an obvious difference is observed among 8 different materials, the inherent deformation of SUS304 stainless steel is larger than the other materials. This should be attributed to the differences of material properties (such as yield stress, thermal expansion coefficient) among 8 different materials.

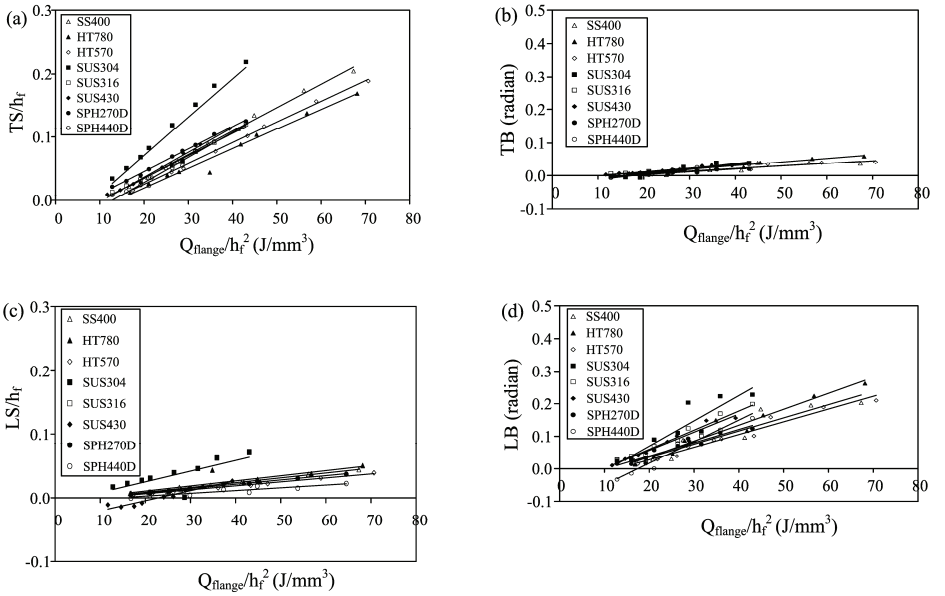

Figure 13: Inherent deformation of flange versus Q/h^2 (a) Transverse shrinkage, (b) Transverse bending, (c) Longitudinal shrinkage, and (d) Longitudinal bending

Fig.14 shows the computational results of inherent deformation in the web of fillet welded T-joint. The inherent deformation is relatively small in the web. The welding heat input parameter (Q_{web}/h_w^2) has little effect on the magnitude of inherent

deformation. Longitudinal bending (LB) is relative large among the four inherent deformation components. It means that longitudinal bending distortion is prone to happen in the web when welding heat input parameter (Q_{web}/h_w^2) is in the range of 10–35 J/mm^3.

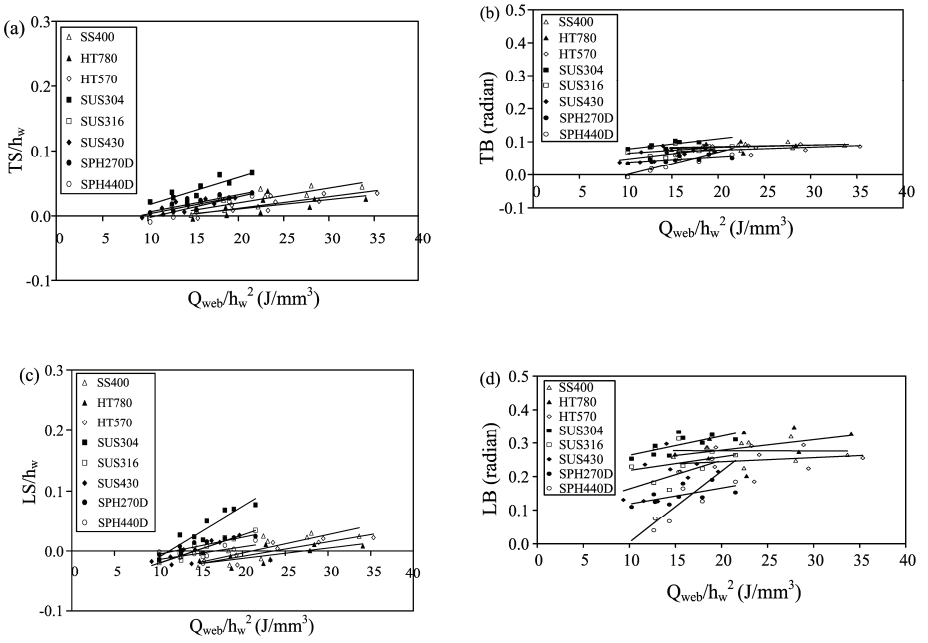

Figure 14: Inherent deformation of web versus Q/h^2 (a) Transverse shrinkage, (b) Transverse bending, (c) Longitudinal shrinkage, and (d) Longitudinal bending

5 Conclusions

According to results obtained in the present work, the conclusions can be summarized as follows:

1. Welding distortion can be reasonable predicted by highly efficient ISM in fillet welded T-joints. The prediction results are in good agreement with the experimental results.

2. The prediction procedure of inherent deformation is developed. The inherent deformations of fillet welded T-joints can be evaluated by ISM combined inverse analysis. Using inherent deformation, welding distortion can be predicted by elastic-shell model.

3. A database of inherent deformation based on 8 different materials in fillet welded T-joints is addressed. The inherent deformation in the flange linearly increases with the increase of welding heat input parameter. Transverse shrinkage and longitudinal bending distortion are prone to happen in the fillet welded thin plate T-joints. The welding heat input parameter has little effect on the inherent deformation in the web.

4. In special welding condition, material properties play an important role on inherent deformation. The inherent deformation of SUS304 is larger than the other materials.

Acknowledgement: The authors would like to thank the Hitachi Ltd. for supplying the experimental results in this study. The results were dedicated to "Survey and research on building welding inherent deformation database and data generation", which was supported by the New Energy and Industrial Technology Development Organization (NEDO).

References

Alaimo, A.; Milazzo, A.; Orlando, C. (2008): Global/Local FEM-BEM stress analysis of damaged aircraft structures. *CMES: Computer Modelling in Engineering and Sciences*, vol. 36, no. 1, pp. 23–41.

Camilleri, D.; Gray, T. G. F. (2005): Computational efficient welding distortion simulation techniques. *Modelling and Simulation in Materials Science and Engineering*, vol. 13, no. 8, pp. 1365–1382.

Camilleri, D.; Comlekci, T.; Gray, T. G. F. (2005): Computational prediction of out-of-plane welding distortion and experimental investigation. *The Journal of Strain Analysis for Engineering Design*, vol. 40, no. 2, pp. 161–176.

Camilleri, D.; Mollicone, P.; Gray, T. G. F. (2006): Alternative simulation techniques for distortion of thin plate due to fillet-welded stiffeners. *Modelling and Simulation in Materials Science and Engineering,* vol. 14, no. 8, pp. 1307–1327.

Deng, D.; Liang, W.; Murakawa, H. (2007): Determination of welding deformation in fillet-welded joint by means of numerical simulation and comparison with experimental measurements. *Journal of materials processing technology*, vol. 183, no. 2–3, pp. 219–225.

Deo, M. V.; Michaleris, P.; Sun, J. (2003): Prediction of buckling distortion of welded structures. *Science and Technology of Welding and Joining*, vol. 8, no. 1, pp. 55–61.

Dong, P. (2005): Residual stresses and distortion in welded structure: a perspective for engineering application. *Science and Technology of Welding and Joining*, vol. 10, no. 4, pp. 389–398.

Lindgren, L. E. (2001a): Finite element modeling and simulation of welding part 1: increased complexity. *Journal of Thermal Stresses*, vol. 24, no. 2, pp. 141–192.

Lindgren, L. E. (2001b): Finite element modeling and simulation of welding part 2: improved material modeling. *Journal of Thermal Stresses*, vol. 24 no. 2, pp. 195–231.

Lindgren, L. E. (2001c): Finite element modeling and simulation of welding part 3: efficiency and integration. *Journal of Thermal Stresses*, vol. 24, no. 2, pp. 305–334.

Liang, W.; Sone, S. J.; Tejima, M.; Serizawa, H.; Murakawa, H. (2004): Measurement of inherent deformation in typical weld joints using inverse analysis (part I) inherent deformation of bead on welding. *Transactions of JWRI*, vol. 33, no. 1, pp. 45–51.

Liang, W.; Deng, D. A.; Murakawa, H. (2005): Measurement of inherent deformation in typical weld joints using inverse analysis (part 2) Prediction of welding distortion of large structures. *Transactions of JWRI*, vol. 34, no.1, pp. 113–123.

Ma, N. X.; Ueda, Y.; Murakawa, H.; Maeda, H. (1995): FEM analysis of 3-D welding residual stresses and angular distortion in T-type fillet welds. *Transactions of JWRI*, vol. 24, no. 2, pp. 115–122.

McDILL, J. M. J.; Oddy, A. S.; Goldak, J. A.; Bennison, S. (1990): Finite element analysis of weld distortion in carbon and stainless steels. *Journal of strain analysis*, vol. 25, no. 1, pp. 51–53.

Michaleris, P.; DeBiccari, A. (1997): Prediction of welding distortion. *Welding Journal*, vol. 76, no. 4, pp. 172s–181s.

Murakawa, H. (2007): Computational welding mechanics and concept of inherent strain for industrial applications. *Materials Science Forum*, vol. 539–43 no. 1, pp. 181–186.

Nishikawa, H.; Serizawa, H.; Murakawa, H. (2007): Actual application of FEM to analysis of large scale mechanical problems in welding. *Science and Technology of Welding and Joining*, vol. 12, no. 2, pp. 147–152.

Oishi, A.; Yoshimura, S. (2008): Finite element analyses of dynamic problems using graphics hardware. *CMES: Computer Modelling in Engineering and Sciences*, vol. 25, no. 2, pp. 115–131.

Raju, I. S.; Glaessgen, E. H.; Mason, B. H.; Krishnamurthy, T.; Davila, C. G. (2007): Structural analysis of the right rear lug of American airlines flight 587.

CMES: Computer Modelling in Engineering and Sciences, vol. 22, no. 1, pp. 1–30.

Satoh, K.; Terasaki, T. (1976): Effect of welding conditions on welding deformations in welded structural materials. *Journal of the Japanese Welding Society*, vol. 45, no. 4, pp. 302–308. (In Japanese)

Seo, S. I.; Jang, C. D. (1999): A study on the prediction of deformations of welded ship structures. *Journal of Ship Production*, vol. 15 no. 2, pp. 73–81.

Takeda, Y. (2002): Prediction of butt welding deformation of curved shell plates by inherent strain method. *Journal of Ship Production*, vol. 18, no. 2, pp. 99–104.

Terasaki, T.; Ishimura, T.; Matsuishi, K.; Akiyama, T. (2002): Study on longitudinal shrinkage of bead-on-plate. *Journal of the Japanese Welding Society*, vol. 20, no. 1, 136–142. (In Japanese)

Teng, T. L.; Fung, C. P.; Chang, P. H.; Yang, W. C. (2001): Analysis of residual stress and distortion in T-joint fillet welds. *International Journal of pressure vessels and piping*, vol. 78, no. 8, pp. 523–538.

Tsai, C. L; Park, S. C.; Cheng, W. T. (1999): Welding distortion of a thin-plate panel structure. *Welding Journal*, vol. 78, no. 5, pp. 157s–165s.

Ueda, Y.; Fukuda, K.; Tanigawa, M. (1979): New measuring method of three dimensional residual stresses based on theory of inherent strain. *Transactions of JWRI*, vol. 8, no. 2, pp. 249–256.

Vega, A.; Rashed, S.; Tango, Y.; Ishiyama, M.; Murakawa, H. (2008): Analysis and Prediction of Multi-Heating Lines Effect on Plate Forming by Line Heating. *CMES: Computer Modelling in Engineering and Sciences*, vol. 28, no. 1, pp. 1–14.

Yuan, M. G.; Ueda, Y. (1996): Prediction of residual stress in welded T- and I-Joints using inherent strains. *Journal of Engineering Materials and Technology*, vol. 118, no. 4, pp. 229–234.

Zaeem, M. A.; Nami, M. R.; Kadivar, M. H. (2007): Prediction of welding buckling distortion in a thin wall aluminum T joint. *Computational Materials Science*, vol. 38, no. 4, pp. 588–594.

Zhang, L. J.; Zhang, J. X.; Serizawa, H.; Murakawa, H. (2007): Parametric studies of welding distortion in fillet welded structure based on FEA using iterative substructure method. *Science and Technology of Welding and Joining*, vol. 12, no.8, pp. 703–707.

Zhu, X. K.; Chao, Y. J. (2002): Effects of temperature-dependent material properties on welding simulation. *Computers and Structures*, vol. 80, no. 11, pp. 967–976.